Parity-time and anti-parity-time states of Bragg gratings and their representation in spherical coordinates

Hao, Tianyi; Cheben, Pavel; Schmid, Jens H.; Berini, Pierre

Publisher's version / Version de l'éditeur:

https://doi.org/10.1364/OE.542182

Optics Express, 32, 26, p. 45521, 2024-12-03

Research Article Vol. 32, No. 26 / 16 Dec 2024 / Optics Express 45521
Optics EXPRESS

Parity-time and anti-parity-time states of Bragg gratings and their representation in spherical coordinates

TIANYI HAO,[1,2] PAVEL CHEBEN,[2,3] JENS H. SCHMID,[3] AND PIERRE BERINI[1,2,4,*]

[1]School of Electrical Engineering and Computer Science, University of Ottawa, Ottawa, Ontario K1N 6N5, Canada
[2]Center for Research in Photonics, University of Ottawa, Ottawa, Ontario K1N 5N6, Canada
[3]National Research Council Canada, Ottawa, ON K1A 0R6, Canada
[4]Department of Physics, University of Ottawa, Ottawa, Ontario K1N 6N5, Canada
[*]pberini@uottawa.ca

Abstract: Parity-time (PT) symmetry and anti-PT symmetry are two interesting types of non-Hermitian Hamiltonian systems. We propose a spherical graphical representation to concisely capture the (anti-)PT symmetry design space of Bragg gratings having phase-shifted real and imaginary refractive index perturbations. A general Bragg grating perturbation function is used such that designs can be arbitrarily changed to reach different (anti-)PT symmetric states. Special cases having simplified perturbations are explored, consisting of real index only, imaginary index only, and perturbations reaching (anti-)PT symmetry unbroken, broken, and exceptional point states. The evolution of the PT states of Bragg gratings and their interesting and unique properties lead to potential applications in sensing and lasing.

1. Introduction

Non-Hermitian Hamiltonians have continuously attracted attention from researchers interested in open systems [1]. A non-Hermitian Hamiltonian $\mathcal{H}$ is Parity-Time (PT) symmetric or anti-PT symmetric if it commutes or anticommutes with the $\mathcal{PT}$ operator: $[\mathcal{H}, \mathcal{PT}] = 0$ or $\{\mathcal{H}, \mathcal{PT}\} = 0$, respectively, where $\mathcal{P}$ is the parity operator and $\mathcal{T}$ is the time reversal operator [2,3]. The eigenvalues of $\mathcal{H}$ are in general complex, except, if it is (anti-)PT symmetric, in which case its eigenvalues are real - such $\mathcal{H}$ are also termed (anti-)PT symmetry unbroken. $\mathcal{H}$ will be (anti-)PT symmetry broken if its eigenvectors differ from those of the (anti-)$\mathcal{PT}$ operator. At the exceptional point (EP), the eigenvalues of $\mathcal{H}$ become degenerate, and $\mathcal{H}$ transitions from (anti-)PT symmetry unbroken to (anti-)PT symmetry broken (or vice versa).

Consider a non-Hermitian Hamiltonian $\mathcal{H}$, having complex eigenvalues and satisfying [10]:

$$\mathcal{PTH} = e^{2i\theta}\mathcal{HPT} \tag{1}$$

where θ is the phase of an eigenvalue. When $\theta = n\pi$ ($n \in \mathrm{Z}$), we have $\mathcal{PTH} = \mathcal{HPT}$ and the system is PT symmetric. When $\theta = n\pi \pm \pi/2$, we have $\mathcal{PTH} = -\mathcal{HPT}$ and the system is anti-PT symmetric. Cases where θ takes on other values correspond to non-Hermitian Hamiltonians that are neither PT symmetric nor anti-PT symmetric.

Given the similarity of the single-particle Schrödinger equation to the paraxial scalar wave equation, the concepts of (anti-)PT symmetry carry over to optical fields by analogy, leading to novel device concepts, *e.g.*, related to lasing [4], sensing [5], and unidirectional propagation [6]. By adjusting the gain, loss and coupling constant in waveguide structures, different PT symmetric states can be accessed, inspiring numerous implementations, including micro-ring resonators, directional couplers, and Bragg gratings to realize functions such as generating vortex beams [7],

#542182 https://doi.org/10.1364/OE.542182
Journal © 2024 Received 18 Sep 2024; revised 9 Nov 2024; accepted 11 Nov 2024; published 3 Dec 2024

Optics EXPRESS

unidirectional reflection [8], coherent perfect absorption [9], chiral polarizer [10] and coupled lasers based on anyonic PT symmetry [11].

In this paper, we consider Bragg gratings having real and imaginary index perturbations as non-Hermitian systems and the evolution of (anti-)PT symmetric states with design. A spherical representation of the Bragg grating design space, mapped to the (anti-)PT symmetric state of the system, is proposed as a design aid in Section 2. Some special cases such as an extreme PT symmetry broken grating, an extreme PT symmetry unbroken grating, and EP gratings where (anti-)PT symmetry breaks down, are presented and analyzed in Section 3. Applications and realistic designs are discussed Section 4, followed by concluding remarks in Section 5

2. Spherical representation of Bragg grating design space

We consider a Bragg grating with gain and loss, and coupling between the forward and backward propagating modes, for which:

$$n(z) = n_{\text{ave}} + \Delta n_r \sin\left(\frac{2\pi}{\Lambda} z\right) + \mathrm{j}\Delta n_{\text{i}} \cos\left(\frac{2\pi}{\Lambda} z + \theta\right) \tag{2}$$

where $n(z)$ is the refractive index distribution of the Bragg grating along the z (propagation) direction, n_{ave} is the average uniform complex refractive index, Δn_r and Δn_{i} are the strength of the real and imaginary index perturbations, Λ is the period of the grating, and θ is an additional phase offset between the real and imaginary index perturbations. Note that for $\theta = 0$, the real and imaginary perturbations are offset along z by $\pi/2$. In Eq. (2), n_{ave} and Λ satisfy $= m\lambda_B/|2n_{ave}|$, where m is the diffraction order, and λ_B is the Bragg wavelength. Note that sinusoids were used in Eq. (2) to describe the periodic perturbations, but the model can describe many types of grating structures represented by other periodic functions, *e.g.*, rectangular perturbations.

θ in Eq. (2) is identical to θ in Eq. (1). A grating is PT symmetric for $\theta = n\pi$ ($n \in \mathrm{Z}$) and anti-PT symmetric for $\theta = n\pi \pm \pi/2$. In addition to these cases, gratings having other values of θ are classified as anyonic PT symmetric. Furthermore, the system is in a (anti-)PT symmetry unbroken state if $\Delta n_r > \Delta n_{\text{i}}$, in a (anti-)PT symmetry broken state if $\Delta n_r < \Delta n_{\text{i}}$, and at the EP if $\Delta n_r = \Delta n_{\text{i}}$. A conventional lossless passive Bragg grating [12] has $\Delta n_{\text{r}} \gg \Delta n_{\text{i}} = 0$ and corresponds to a grating in the PT symmetry unbroken state. Index-coupled DFB lasers [13] have $\theta = 0$ and $\Delta n_{\text{r}} \gg \Delta n_{\text{i}} > 0$, and also correspond to structures the PT symmetry unbroken state. Gratings in a PT symmetry broken state produce asymmetric reflectance, *i.e.*, a reflectance that differs depending on which port is used as the input. Such structures have been applied to lasing, reflection and switching applications [14–16]. The Fourier representation of the index perturbation of such gratings has an asymmetric sideband spectrum [17]. Perfect unidirectional reflection (or unidirectional transparency) can be achieved precisely at the EP because the index perturbation spectrum has only a single sideband.

Returning to Eq. (2), there are three important ingredients to consider: the phase θ constrained to $[0,\ 2\pi]$ (mod(2π)), the perturbation amplitudes Δn_r and Δn_{i} (both having the same period Λ), and n_{ave} which along with Λ determines the central (Bragg) wavelength of the grating. All three ingredients are independent from each other and can be used to define a spherical space capturing designs that follow Eq. (2). This general perturbation distribution can be represented by a sphere of radius $\mathrm{r} = |n_{\text{ave}}|$, azimuthal coordinate θ, and polar coordinate $\varphi = \text{acos}((\Delta n_i - \Delta n_r)/(\Delta n_i + \Delta n_r))$, as sketched in Fig. 1(a). The center of the sphere is located at the origin of the coordinate system. The radius r determines the size of the sphere following $|n_{\text{ave}}|$. The azimuthal angle θ corresponds directly to θ in Eqs. (1 and 2), and determines whether the system is PT symmetric or anti-PT symmetric. The polar angle φ depends on Δn_r and Δn_{i} and determines whether the system is in a broken or unbroken state. All possible (anti-)PT symmetric states can then be illustrated on a sphere as shown in Fig. 1(a). In Fig. 1(a), the yellow ring corresponds to anti-PT symmetric gratings ($\theta = n\pi \pm \pi/2$), whereas the green ring corresponds

Optics EXPRESS

to PT symmetric gratings ($\theta = n\pi$). The northern hemisphere ($\varphi \in [0, \pi/2)$) has $\Delta n_r < \Delta n_i$, which corresponds to symmetry broken states, whereas the southern hemisphere ($\varphi \in (\pi/2, \pi]$) corresponds to symmetry unbroken states with $\Delta n_r > \Delta n_i$. The equatorial black ring corresponds to $\Delta n_r = \Delta n_i$ and $\varphi = \pi/2$ indicating exceptional points that separate broken and unbroken states. The north pole ($\varphi = 0$) corresponds to $\Delta n_r = 0$ which yield gratings with an imaginary index perturbation, whereas gratings at the south pole ($\varphi = \pi$) have a real index perturbation with $\Delta n_i = 0$. We can think of the north pole (imaginary perturbation only) as defining gratings in an extreme (anti-)PT symmetry broken state, and the south pole (real perturbation only) as defining gratings in an extreme (anti-)PT symmetry unbroken state.

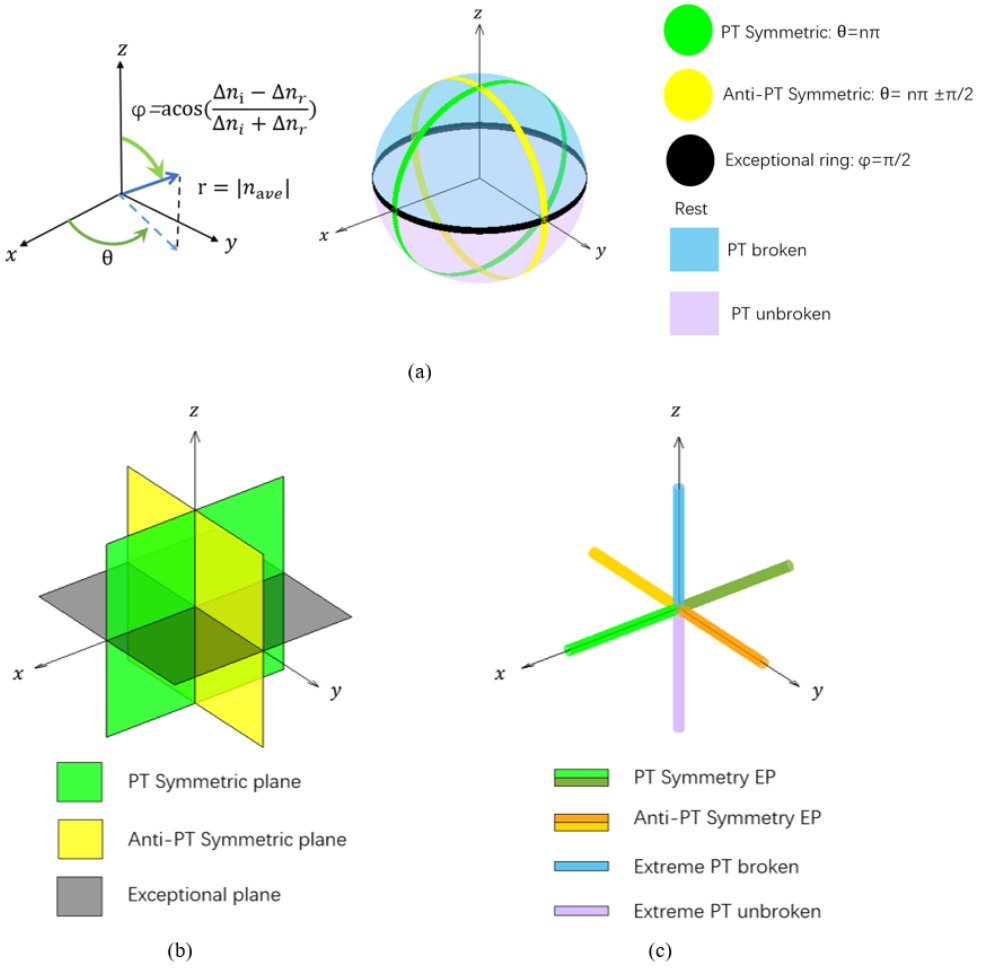

Fig. 1. (a) Spherical representation of Eq. (2) with regions of the sphere identifying (anti-)PT symmetric states. (b) Cartesian planes and (c) axes intersecting the spherical space, highlighting (anti-)PT symmetric states.

More generally, the three rings on the sphere representing anti-PT symmetric, PT symmetric and EP states define three Cartesian planes that also identify these states as shown in Fig. 1(b): the $x = 0$ plane captures anti-PT symmetric states, the $y = 0$ plane captures PT symmetric states, and the plane $z = 0$ captures EP states. The intersections of these planes, shown in Fig. 1(c), correspond to the Cartesian axes on which gratings exhibit interesting characteristics. A grating on the x-axis is at a PT symmetry EP and produces a unidirectional reflectance (the

Optics EXPRESS

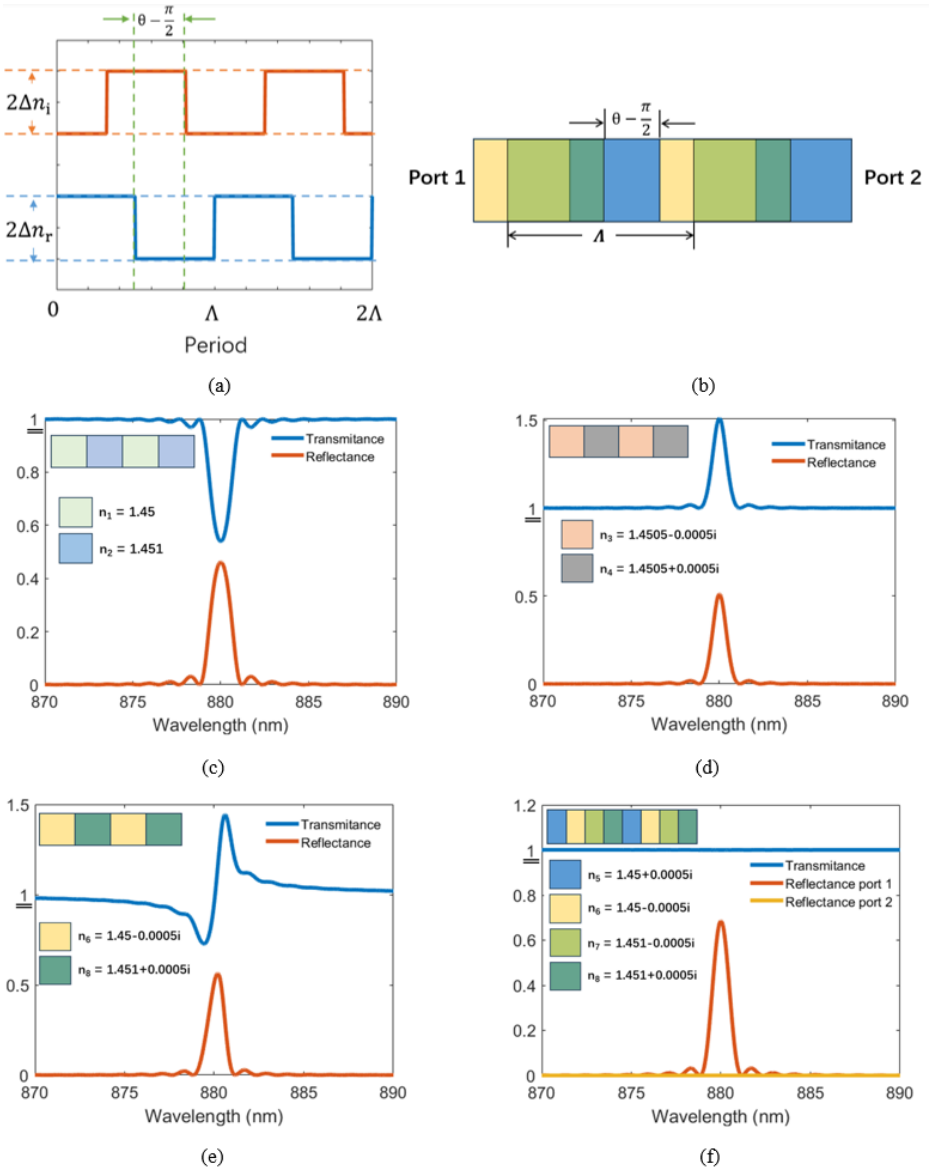

Fig. 2. (a) Functional representation and (b) sketch of a rectangular refractive index perturbation for a non-Hermitian Bragg grating implemented as a dielectric stack. Transmittance and reflectance spectra of example Bragg grating designs with their dielectric structure. (c) Extreme (anti-)PT symmetry unbroken state (south pole). (d) Extreme (anti-)PT symmetry broken state (north pole). (e) Anti-PT symmetry EP. (f) PT symmetry EP. (Note the different *y*-axis limits used in (c)-(d)).

Optics EXPRESS

positive and negative portions of the x-axis correspond to gratings that produce a reflectance from different ports). A grating on the y-axis is at an anti-PT symmetry EP and produces a distorted reflectance peak and one single strong oscillation in its transmittance (the positive and negative portions of the y-axis correspond to gratings that have different wavelength shift directions and opposite oscillation shape). A grating on the positive z-axis is in an extreme (anti-)PT symmetry broken state (imaginary perturbation only) and produces a transmittance peak at the center wavelength. A grating on the negative z-axis is in an extreme (anti-)PT symmetry unbroken state (real perturbation only) and produces a conventional grating response.

3. Results and discussion

Figure 2(a) plots a rectangular distribution of real and imaginary index perturbations following the model of Eq. (2), whereas Fig. 2(b) illustrates a corresponding possible implementation as a periodic dielectric stack with each period comprised of four layers. Figures 2(c) to 2(d) plot the transmittance (T) and reflectance (R) of example gratings operating in four special states: extreme (anti-)PT symmetry unbroken, extreme (anti-)PT symmetry broken, anti-PT symmetry EP, and PT symmetry EP. These states are located at the south pole, north pole, equator with azimuthal angle $\theta = \pm\pi/2$, and equator with azimuthal angle $\theta = 0$ or π on the PT sphere, respectively. The spectra were calculated by the transfer matrix method (TMM) [18], using $n_{ave} = 1.4505$, $\lambda_B = 880$ nm, ~750 grating periods, and specific refractive index values for the dielectric layers constituting each grating stack as given in inset to each figure.

A conventional Bragg grating is usually assumed to have no perturbation in its imaginary refractive index and corresponds to an extreme (anti-)PT symmetry unbroken state located at the south pole of the PT sphere. Such gratings produce a strong back reflection (R) at the center wavelength, with a corresponding dip in transmittance (T), as shown in Fig. 2(c). The reason why the transmission and reflection do not reach 0 and 1, respectively, at the Bragg wavelength is because the perturbation is weak and the number of periods in our model is finite. When the average gain ($\mathrm{Im}(n_{\mathrm{ave}})$) of the grating is small (for operation near the south pole), the sum of the reflectance and transmittance remains flat over a broad bandwidth and satisfies $T + R = 1$ for $\mathrm{Im}(n_{\mathrm{ave}}) = 0$.

At the north pole of our spherical representation, a Bragg grating corresponds to an extreme (anti-)PT symmetry broken state with no real refractive index perturbation. These gain-coupled gratings can produce a strong back reflection but also strong amplification in transmission near the center wavelength, as shown in Fig. 2(d). This is because the forbidden band in extreme (anti-)PT symmetry unbroken gratings (south pole) vanishes in extreme (anti-)PT symmetry broken gratings (north pole) [19]. The difference between the transmittance and reflectance (T-R) is close to constant over the resonant wavelength range ($T - R = 1$ for $\mathrm{Im}(n_{\mathrm{ave}}) = 0$).

The transmittance and reflectance behavior of anti-PT symmetric EP gratings are peculiar compared to gratings in other states. Such gratings have $\Delta n_r = \Delta n_{\mathrm{i}}$ and $\theta = n\pi + \pi/2$, so they have the same magnitude of perturbation in the real and imaginary index and they are in phase (*cf.* Equation (2) with $\theta = \pi/2$). In Fig. 2(e), the reflection peak is shifted slightly from the center wavelength (red shifted if n is even, blue shifted if n is odd), and the transmittance has a peak and a valley near the center wavelength (a valley at wavelengths shorter than the center wavelength and a peak at wavelengths longer than the center wavelength if n is even, and vice versa if n is odd). The transmittance at the center wavelength is equal to that away from resonance ($T = 1$ at the center wavelength if $\mathrm{Im}(n_{\mathrm{ave}}) = 0$). The behaviour of anti-PT symmetric EP gratings has never been reported before.

PT symmetric EP gratings [20] produce unidirectional reflection, as shown in Fig. 2(f). Compared with the three other cases, this grating produces a strong back reflection (from port 1) without peak shifting from the center wavelength. The port from which reflection occurs

Optics EXPRESS

depends on whether n is even or odd (in $\theta = n\pi$). The transmittance of this state is flat, without any oscillations as for other PT states ($T = 1$ over the wavelength range if $\mathrm{Im}(n_{\mathrm{ave}}) = 0$).

Material dispersion was neglected in these calculations because the weak perturbation produced by the gratings yield a narrow bandwidth (~1.5 nm). All four gratings representing the PT states presented in Fig. 2 have a similar bandwidth because of the close and small magnitude of the real and imaginary index perturbations.

The distribution of the electric field magnitude over two periods of each grating of Fig. 2 is shown in Fig. 3, computed using the eigenmode expansion method (EME) [21]. The refractive indices for the dielectric stacks of Fig. 3 are the same as the corresponding ones of Fig. 2.

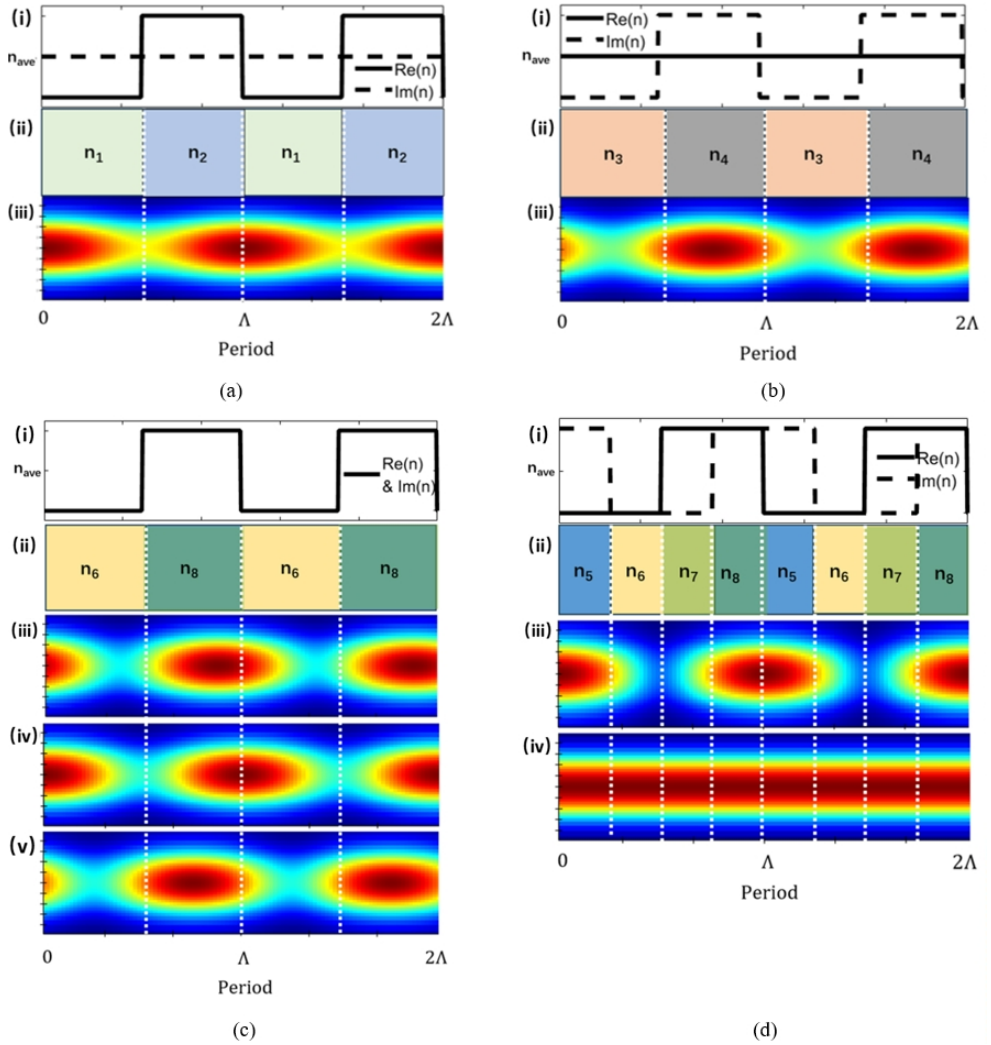

Fig. 3. (i) Index perturbations and (ii) dielectric stack over two periods of the corresponding example gratings of Fig. 2. (iii) to (v) Electric field distribution, for light input into port 1, except for part (d)(iv) where light is input into port 2. (a) Extreme (anti-)PT symmetry unbroken state (south pole) at (iii) Bragg wavelength. (b) Extreme (anti-)PT symmetry broken state (north pole) at (iii) Bragg wavelength. (c) Anti-PT symmetry EP at (iii) Bragg wavelength, (iv) transmission valley, and (v) transmission peak. (d) PT symmetry EP when light is (iii) input into port 1, and (iv) input into port 2.

Optics EXPRESS

Except for the PT symmetric EP grating excited at port 2 (Fig. 3(d)iv), all other cases result in an explicitly periodic field distribution. The extreme (anti-)PT symmetry unbroken (south pole) grating shown in Fig. 3(a) has a field distributed over the grating period, whereas the extreme (anti-)PT symmetric broken (north pole) grating has a field localized to the gain regions as shown in Fig. 3(b). There is a $\pi/2$ ($\Lambda/4$) shift in the field distribution between these extreme unbroken and broken states, which originates from the form assumed for the dielectric stack (Fig. 2(a)), which follows the model of Eq. (2) written with this inherent shift between the real and imaginary parts (*cf.* sin and cos terms).

The field distribution in the anti-PT symmetric EP state grating, shown in Fig. 3(c), is as peculiar as its spectrum. At the Bragg wavelength, the field is mainly localized at the midpoint between maximum magnitude locations of extreme (anti-)PT unbroken and extreme (anti-)PT broken states (Fig. 3(c)iii). However, when the wavelength shifts away from the center wavelength, the field distribution approaches that of the extreme (anti-)PT unbroken state at the wavelength of the transmission valley (Fig. 3(c)iv *vs*. Figure 3(a)iii), and that of the extreme (anti-)PT symmetry broken state at the wavelength of the transmission peak (Fig. 3(c)v *vs*. Figure 3(b)iii).

Because of the unidirectional reflection property of PT symmetric EP gratings, the field distributions for light input into ports 1 and 2 differ significantly. The field distributions are periodic for light input into port 1 (Fig. 3(d)iii) but uniform for light input into port 2 (Fig. 3(d) iv). The field distribution corresponding to the reflectance peak into port 1 is mainly localized in the gain regions of the grating, as in the extreme (anti-)PT symmetry broken state Fig. 3(b), along the interface between the different real index portions of the grating period as in the extreme (anti-)PT symmetry unbroken state of Fig. 3(a).

Slight changes in design relative to these special locations on the PT sphere can significantly alter device performance. For instance, the reflection ratio from the ports can be adjusted, the degree of wavelength reflection peak shift, and the amount of gain or the filtering properties in transmission can be controlled by changing the polar and azimuthal angles.

In the previous examples (Fig. 2), an average gain of about 0 with weak perturbation was assumed such that the grating produced a reflectance less than 1, and therefore will not lase. However, if a high gain is assumed, $R > 1$, and the system can lase. This case is now considered by setting $\mathrm{Im}(n_{\mathrm{ave}}) = 0.0007$.

Figure 4(a) shows the responses of a conventional DFB laser design where $\Delta n_{\mathrm{r}} \gg \Delta n_{\mathrm{i}} > 0$. Although the perturbation of the imaginary part is much weaker than the real part, the state of the DFB laser is shifted away from the extreme (anti-)PT symmetry unbroken state (south pole). Compared to the responses of the extreme (anti-)PT symmetry unbroken grating in Fig. 2(c), a DFB laser design has a shifted center wavelength in its reflectance and stronger oscillations in its transmittance.

If the weak imaginary perturbation assumed in the DFB laser is absent, but the average gain or the real index perturbation are strong, two similar and strong reflection peaks are observed in the reflectance and transmittance responses, as shown in Fig. 4(b). This double-peak characteristic can only be observed in an extreme (anti-)PT symmetry unbroken state grating (south pole) with high Δn_{r} or high $\mathrm{Im}(n_{\mathrm{ave}})$. Once the PT state evolves from extreme (anti-)PT symmetry unbroken, the similarity in the two peaks breaks and the spectrum approaches that of the conventional DFB laser (Fig. 4(a)).

The spectral response of a grating that doesn't belong to any special state on the PT sphere is also plotted in Fig. 4(c). We can see interesting features in its transmittance and reflectance responses, such as asymmetric reflectance, oscillating transmittance, and a shifted peak reflectance wavelength. This behavior highlights the flexible nature of the grating design captured by the model of Eq. (2) and the PT sphere.

Optics EXPRESS

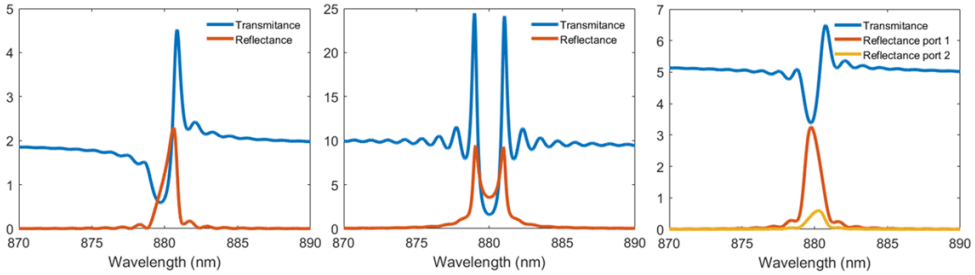

Fig. 4. Transmittance and reflectance spectra of example grating designs. (a) PT symmetric state of a conventional DFB laser structure. (b) Extreme (anti-)PT symmetry unbroken state (south pole on the PT sphere) with high average gain or large Δn_r. (c) Arbitrary state located away from the x, y and z planes of Fig. 1(b).

4. Possible implementation

A Bragg grating waveguide structure that perturbs the real and imaginary parts of the effective index with a relative phase shift (*cf.* Equation (2) or Fig. 2(a)), that is represented by a non-Hermitian Hamiltonian, and that covers the entire PT sphere, is presented in Fig. 5. The structure incorporates a long-range surface plasmon polariton (LRSPP) metal waveguide grating [22], with

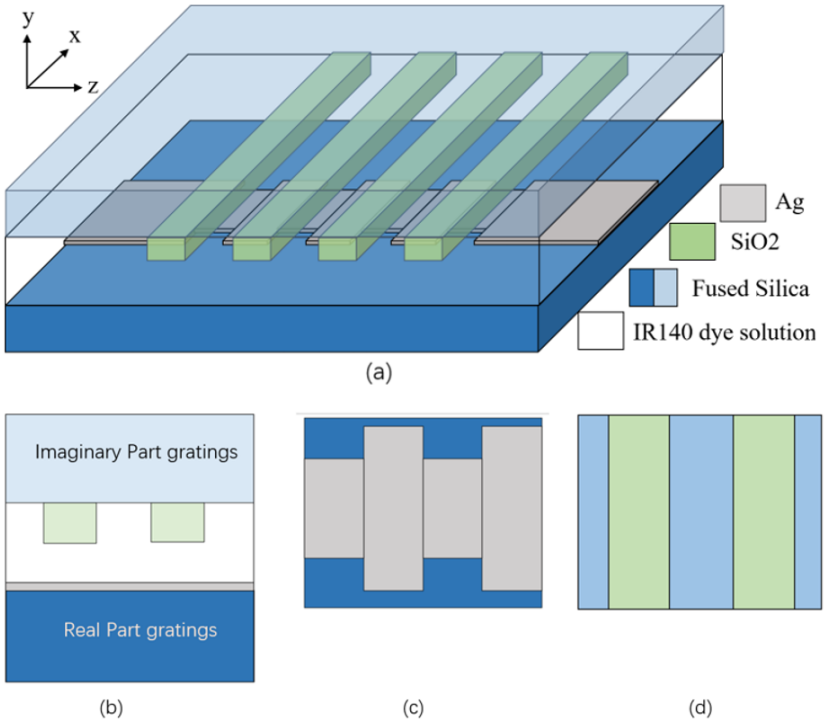

Fig. 5. (a) Schematics of a Bragg grating that can reach any state on the PT sphere. (b) Side view of the two-layer structure, (c) top view of the lower layer bearing a metal step-in-width grating providing real index perturbation, and (d) bottom view of the upper layer providing imaginary index perturbation.

Optics EXPRESS

an overlaid and shifted SiO_2 grating of the same period, covered and infiltrated by a dye solution, *e.g.*, IR-140. The metal stripe waveguide is patterned as a step-in-width structure on a fused silica substrate and provides perturbations in the real part of the effective index. The IR-140 dye solution can produce gain at 880 nm when pumped optically near 820 nm [23]. The solvent for the dye is selected to produce a real part of refractive index equal to that of SiO_2 at room temperature [23]. Combining the dye solution with the SiO_2 grating and the metal waveguide grating, as sketched in Fig. 5(b), provides the imaginary perturbation. Effective refractive indices for this structure at extreme (anti-)PT (un)broken and (anti-)PT EP states close to those given in Fig. 2 are achievable. In this design, the real index perturbation Δn_r is dependent on the metal waveguide grating design, and the refractive index of the dye solution which is adjustable with temperature [24]. The imaginary index perturbation Δn_i is dependent on the separation between the two layers (Fig. 5(b)), and the gain provided by the dye molecules which is adjustable with the pump light power. It is an advantage that real and imaginary perturbations are independent in this structure, as this provides more flexibility to control the PT state of the grating. Because the real and the imaginary parts of the grating are on two different layers, and the solution between them can be flowed, the relative position of the two layers can be adjusted to modify the phase θ between the real and imaginary gratings. This structure is experimentally realizable and capable of spanning the full PT sphere.

5. Conclusions

We studied the transmission and reflection properties of non-Hermitian Bragg gratings accessing different PT states. To conveniently visualize the (anti-)PT symmetry design space of Bragg gratings with shifted real and imaginary index perturbations, we proposed a spherical graphical representation. This spherical graphical construction could be mathematically extended to other PT systems with gain/loss and coupling between modes, like directional couplers, coupled micro-rings, and a micro-ring coupled to a grating, for which a 2×2 Hamiltonian can be constructed to model their behavior. When a Bragg grating evolves from the extreme (anti-)PT symmetry unbroken state to the extreme (anti-)PT symmetry broken state, its transmittance near the center wavelength changes from a stop band to an amplifying passband. Unidirectional reflection, which is observed at a PT symmetry EP, is compromised as soon as the PT state evolves from this point. Furthermore, the center wavelength has been observed to red- or blue-shift, which is potentially relevant to a wavelength tunable laser design. The proposed PT sphere should help designers configure gratings for operation in specific states. Specially, it has helped uncover a novel anti-PT symmetry EP grating that has a peculiar (oscillatory) transmission response with a shifted reflection peak. Furthermore, gratings based on the concepts of (anti-)PT symmetry and exceptional points are sensitive to external perturbations, making the structures well-suited to sensor or tunable laser applications.

Funding. Natural Sciences and Engineering Research Council of Canada; National Research Council Canada.

Disclosures. The authors declare no conflicts of interest.

Data availability. Data underlying the results presented in this paper may be obtained from the authors upon reasonable request.

References

1. A. Li, H. Wei, M. Cotrufo, *et al.*, "Exceptional points and non-Hermitian photonics at the nanoscale," Nat. Nanotechnol. **18**(7), 706–720 (2023).
2. C. M. Bender, "Introduction to PT-symmetric quantum theory," Contemp. Phys. **46**(4), 277–292 (2005).
3. Y. L. Fang, J. L. Zhao, Y. Zhang, *et al.*, "Experimental demonstration of coherence flow in PT- and anti-PT-symmetric systems," Commun. Phys. **4**(1), 223 (2021).
4. V. B. Perrière, Q. Gaimard, H. Benisty, *et al.*, "Electrically injected parity-time symmetric distributed feedback laser diodes (DFB) for telecom applications," Nanophotonics **10**(4), 1309–1317 (2021).
5. H. Qin, Y. Yin, and M. Ding, "Sensing and induced transparency with a synthetic anti-PT symmetric optical resonator," ACS Omega **6**(8), 5463–5470 (2021).

Optics EXPRESS

6. Y. Choi, C. Hahn, J. W. Yoon, *et al.*, "Extremely broadband, on-chip optical nonreciprocity enabled by mimicking nonlinear anti-adiabatic quantum jumps near exceptional points," Nat. Commun. **8**(1), 14154 (2017).
7. P. Miao, Z. Zhang, J. Sun, *et al.*, "Orbital angular momentum microlaser," Science **353**(6298), 464–467 (2016).
8. T. Hao and P. Berini, "Directional coupling with parity-time symmetric Bragg gratings," Opt. Express **30**(4), 5167–5176 (2022).
9. Y. Sun, W. Tan, H. Q. Li, *et al.*, "Experimental demonstration of a coherent perfect absorber with PT phase transition," Phys. Rev. Lett. **112**(14), 143903 (2014).
10. Y. Wei, Z. H. Zhou, Y. Chen, *et al.*, "Anti-parity-time symmetry enabled on-chip chiral polarizer," Photonics Res. **10**(1), 76–83 (2022).
11. G. Arwas, S. Gadasi, I. Gershenzon, *et al.*, "Anyonic-parity-time symmetry in complex-coupled lasers," Sci. Adv. **8**(22), eabm7454 (2022).
12. A. Othonos, "Fiber bragg gratings," Rev. Sci. Instrum. **68**(12), 4309–4341 (1997).
13. E. Keshmarzi, R. Tait, and P. Berini, "Single-mode surface plasmon distributed feedback lasers," Nanoscale **10**(13), 5914–5922 (2018).
14. H. Benisty, V. B. Perrière, A. Ramdane, *et al.*, "Parity-time symmetric gratings in 1550 nm distributed-feedback laser diodes: insight on device design rules," J. Opt. Soc. Am. B **38**(9), C168–C174 (2021).
15. S. Phang, A. Vukovic, H. Susanto, *et al.*, "Ultrafast optical switching using parity–time symmetric Bragg gratings," J. Opt. Soc. Am. B **30**(11), 2984–2991 (2013).
16. M. Kulishov and B. Kress, "Distributed Bragg reflector structures based on PT-symmetric coupling with lowest possible lasing threshold," Opt. Express **21**(19), 22327–22337 (2013).
17. M. Kulishov, J. M. Laniel, N. Bélanger, *et al.*, "Nonreciprocal waveguide Bragg gratings.," Opt. Express **13**(8), 3068–3078 (2005).
18. S. Jetté-Charbonneau, R. Charbonneau, N. Lahoud, *et al.*, "Bragg Gratings Based on Long-Range Surface Plasmon-Polariton Waveguides: Comparison of Theory and Experiment," IEEE J. Quantum Electron. **41**(12), 1480–1491 (2005).
19. H. Kogelnik and C. Vo Shank, "Coupled-wave theory of distributed feedback lasers," J. Appl. Phys. **43**(5), 2327–2335 (1972).
20. E. K. Keshmarzi, R. N. Tait, and P. Berini, "Spatially nonreciprocal Bragg gratings based on surface plasmons," Appl. Phys. Lett. **105**(19), 191110 (2014).
21. Ansys Lumerical, "MODE - EigenMode Expansion (EME) solver introduction", Lumerical (2021), https://support.lumerical.com/hc/en-us/articles/360034396614-MODE-EigenMode-Expansion-EME-solverintroduction
22. P. Berini, "Long-range surface plasmon polaritons," Adv. Opt. Photonics **1**(3), 484–588 (2009).
23. I. De Leon and P. Berini, "Amplification of long-range surface plasmons by a dipolar gain medium," Nat. Photonics **4**(6), 382–387 (2010).
24. M. Bertolotti, V. Bogdanov, A. Ferrari, *et al.*, "Temperature dependence of the refractive index in semiconductors," J. Opt. Soc. Am. B **7**(6), 918–922 (1990).